Road-Map–Assisted Standoff Tracking of Moving Ground Vehicle Using Nonlinear Model Predictive Control

HYONDONG OH
Loughborough University
Loughborough, United Kingdom

SEUNGKEUN KIM
Chungnam National University
Daejeon, Republic of Korea

ANTONIOS TSOURDOS
Cranfield University
Cranfield, United Kingdom

This paper presents road-map–assisted standoff tracking of a ground vehicle using nonlinear model predictive control. In model predictive control, since the prediction of target movement plays an important role in tracking performance, this paper focuses on utilizing road-map information to enhance the estimation accuracy. For this, a practical road approximation algorithm is first proposed using constant curvature segments, and then nonlinear road-constrained Kalman filtering is followed. To address nonlinearity from road constraints and provide good estimation performance, both an extended Kalman filter and unscented Kalman filter are implemented along with the state-vector fusion technique for cooperative unmanned aerial vehicles. Lastly, nonlinear model predictive control standoff tracking guidance is given. To verify the feasibility and benefits of the proposed approach, numerical simulations are performed using realistic car trajectory data in city traffic.

Manuscript received October 28, 2013; revised June 25, 2014; released for publication September 1, 2014.

DOI. No. 10.1109/TAES.2014.130688.

Refereeing of this contribution was handled by W. Koch.

Authors' addresses: H. Oh, Department of Aeronautical and Automotive Engineering, Loughborough University, Loughborough, Leicestershire, LE11 3TU, United Kingdom; S. Kim, Department of Aerospace Engineering, Chungnam National University, 99 Daehak-ro, Yuseong-gu, Daejeon, 305-764, Republic of Korea (South), E-mail: (skim78@cnu.ac.kr); A. Tsourdos, Institute of Aerospace Science, Cranfield University, Cranfield, MK43 0AL, United Kingdom.

I. INTRODUCTION

Surveillance, and subsequent tracking, of a stationary or moving ground target of interest is one of the important capabilities of UAVs (Unmanned Aerial Vehicles) since it is essential to increase an overall knowledge of the surrounding environment [1–3]. To produce appropriate surveillance data to be used by UAVs, a ground moving target indicator (GMTI) is a well-suited sensor due to its wide coverage and all-weather, day/night, and real-time capabilities [4]. From these sensor data, such as range, azimuth, or elevation of the target with respect to the sensor location (along with appropriate target dynamics), a certain level of accurate estimation could be obtained using conventional filtering techniques. However, as ground target tracking is a challenging problem due to the uncertainty of the target maneuvers, all available information sources should be exploited: its own sensor data, data from other UAVs, and contextual knowledge about the sensor performance and the environment. In other words, information fusion is required to improve the estimation accuracy.

In particular, in many applications for ground target tracking, the majority of ground vehicles are moving on road networks for which topographical coordinates could be known with a certain accuracy. Such road-map information can be used for improving the quality of tracking significantly by constraining the state of the ground target of interest, especially in its position, velocity, and acceleration within the road geometry. This is known as a road-constrained target tracking problem, and there are largely three categories of techniques for making use of the information about the roads. The first one is the postprocessing correction technique, which runs a tracking algorithm first without the road information, and correction is then applied. Tang et al. [5] and Kanchanavally et al. [6] proposed a Bayesian filtering method with the hospitability map, which provides a likelihood for each point proportional to the ability of a target to move at that location. Along with this approach, Kassas et al. [7] added the concept of a synthetic inclination map, which describes how the target will be synthetically inclined to move in different directions with a certain velocity component. The second one is the preprocessing of target state or sensor measurements. Road information is exploited by defining the target state in road coordinates and performing transformations between the road and ground coordinate system to consider the sensor measurements in the filter update step [8, 9]. Herrero et al. [10] proposed the preprocessing of sensor measurements with map restriction. Moreover, they introduced a map-tuned interactive multiple model (IMM) structure, which consists of constant speed, a longitudinal acceleration model, and a curvilinear model incorporating map information. The third one is a constrained filtering framework. Dan et al. [11] proposed Kalman filtering with state equality constraints and used road information as equality constraints. Zhang et al. [12] used a

pseudomeasurement approach, which treats the road constraints as additional fictitious measurements based on the work of Tahk and Speyer [13]. To deal with a road network that has road junctions and crossing of several roads, the variable structure IMM filtering concept was also proposed by [14, 15]. Even though the particle filter might result in better tracking performance depending on the situation, particularly for a highly nonlinear system and non-Gaussian noise as described in [16, 17], it would require a significant computational cost. Since this paper considers the use of small and low-cost UAVs rather than a single UAV with high computation power, this paper mainly uses Kalman filter–based algorithms.

Having estimated target information, UAVs should be able to keep a certain distance from the moving target with prescribed intervehicle angular spacing in order to track it without being noticed and at the same time to acquire accurate target information. The certain relative distance from the target is called the standoff distance, and therefore this approach is known as standoff target tracking. For this standoff tracking problem, Lawrence [18] first proposed the application of Lyapunov vector fields for standoff coordination of multiple UAVs. This Lyapunov vector field guidance (LVFG) was further investigated by Frew et al. [19, 20] and Summers et al. [21] to include phase keeping as well as standoff distance tracking. They invented a decoupled control structure in which the speed and rate of heading change are separately controlled for the standoff distance and phase angle keeping, respectively. Similarly, Kingston et al. [22] used the vector field approach; however, they introduced a sliding mode control and orbit radius change without velocity change for phase-keeping of multiple UAVs. Yoon et al. [3] applied the stabilization of a spherical pendulum to the conical motion of the aircraft motion in order to obtain the standoff tracking guidance commands. Oh et al. [23] used the solution of differential geometry between the UAV and the target, which provides rigorous stability along with its inherent simplicity. Oh et al. [24] also introduced cooperative standoff tracking of groups of multiple targets using Lyapunov vector fields and an online local replanning strategy. Kim et al. [25] applied a receding horizon model–based predictive control by combining heading and speed control in a decentralized manner. Wise and Rysdyk [26] surveyed and compared the different methodologies for standoff tracking: These were the Helmsman behavior, Lyapunov vector field, controlled collective motion, and model predictive control.

This paper presents road-map–assisted standoff tracking of a moving ground vehicle using nonlinear model predictive control (NMPC) based on our previous work [25]. In the previous work, the NMPC method was able to contribute toward acquiring optimal performance in terms of standoff tracking performance and fuel consumption compared with using the existing decoupled guidance structure. However, in this sort of model predictive control, since the prediction of the target movement plays an important role in the tracking performance, this paper focuses on utilizing road-map information to enhance the target estimation accuracy. There are not many works on road-constrained estimation using real road-map data in the literature, and road-constrained estimation has rarely been dealt or combined with target tracking guidance, even though a ground vehicle of interest is moving only on the road in many cases. Having this in mind, this paper firstly proposes a practical road approximation algorithm using constant curvature segments. Secondly, to exploit road information for precise target estimation, nonlinear road-constrained Kalman filtering is applied using a pseudomeasurement approach. Furthermore, to address nonlinearity of road constraints and provide good estimation performance, both an extended Kalman filter (EKF) and unscented Kalman filter (UKF) are implemented along with the state-vector fusion technique for cooperative UAVs. Lastly, nonlinear model predictive control standoff tracking guidance is explained briefly, and numerical simulations with a pair of UAVs are performed using realistic car trajectory data in city traffic in the United Kingdom. In the simulation results, the effect of improved estimation accuracy on the tracking guidance performance is analyzed for both broadly used LVFG and the proposed NMPC guidance.

The overall structure of this paper is given as follows. Section II contains a definition of the UAV dynamic model, the ground target, and the sensor model considered in this study. Section III explains the road-constrained tracking filter design and sensor fusion utilizing the road approximation technique. Section IV explains the decentralized structure, definition of performance index and constraints, and nonlinear model predictive controller design for cooperative standoff tracking. Section V presents numerical simulation results of a standoff tracking scenario using realistic ground vehicle trajectory data. Lastly, conclusions and future works are given in section VI.

II. PROBLEM FORMULATION

A. UAV Dynamic Model

Assuming each UAV has a low-level flight controller such as a stability/controllability augmentation system for heading and velocity hold functions, this study aims to design guidance inputs to this low-level controller for standoff target tracking. Consider a two-dimensional UAV kinematic model [25] as:

$$\begin{pmatrix} \dot{x} \\ \dot{y} \\ \dot{\psi} \\ \dot{v} \\ \dot{\omega} \end{pmatrix} = f(\mathbf{x}, \mathbf{u}) = \begin{pmatrix} v\cos\psi \\ v\sin\psi \\ \omega \\ -\dfrac{1}{\tau_v}v + \dfrac{1}{\tau_v}u_v \\ -\dfrac{1}{\tau_\omega}\omega + \dfrac{1}{\tau_\omega}u_\omega \end{pmatrix} \tag{1}$$

where $\mathbf{x} = (x, y, \psi, v, \omega)^T$ are the inertial position, heading, speed, and yaw rate of the UAV, respectively; τ_v and τ_ω are time constants for considering actuator delay; and $\mathbf{u} = (u_v, u_\omega)^T$ are the commanded speed and turning rate constrained by the following dynamic limits of fixed-wing UAV:

$$|u_v - v_0| \leq v_{max} \tag{2}$$

$$|u_\omega| \leq \omega_{max} \tag{3}$$

where v_0 is the nominal speed of the UAV. The continuous UAV model in (1) can be discretized by Euler integration into:

$$\mathbf{x}_{k+1} = f_d(\mathbf{x}_k, \mathbf{u}_k) = \mathbf{x}_k + T_s f(\mathbf{x}_k, \mathbf{u}_k) \tag{4}$$

where $\mathbf{x}_k = (x_k, y_k, \psi_k, v_k, \omega_k)^T$, $\mathbf{u}_k = (u_{vk}, u_{\omega k})^T$, and T_s is a sampling time.

B. Ground Target and Sensor Model

General target tracking filters have traditionally been developed for monitoring aerial targets such as airplanes, missiles, and so on. Although ground vehicles move with much lower speeds than aerial targets, they often perform irregular stop-and-go maneuvers with a much smaller turn radius. The constant-velocity model usually used for radar target tracking is thus unsuitable for tracking ground vehicles, and hence an acceleration or jerk model is a more suitable candidate. Considering general car behavior, because the jerk is not negligible, but the acceleration can be best modelled using a piecewise constant profile over a specific duration of time, a good model to apply to the tracking of ground targets is the acceleration dynamics model [25]. This acceleration model defines the target acceleration as a correlated process with a decaying exponential autocorrelation function, which means if there is a certain acceleration at a time t, then it is likely to be correlated via the exponential at a time instant $t + \tau$. A discretized system equation for this acceleration model for a ground vehicle is thus expressed in the form:

$$x_k^t = F_k \mathbf{x}_{k-1}^t + \eta_k \tag{5}$$

where the state vector is $\mathbf{x}_k^t = (x_k^t, \dot{x}_k^t, \ddot{x}_k^t, y_k^t, \dot{y}_k^t, \ddot{y}_k^t)^T$, and where η_k is a process noise, which represents the acceleration characteristics of the target. The state transition matrix F_k is given by:

$$F_k = \begin{bmatrix} 1 & T_s & \Phi & 0 & 0 & 0 \\ 0 & 1 & \dfrac{(1 - e^{-\alpha T_s})}{\alpha} & 0 & 0 & 0 \\ 0 & 0 & e^{-\alpha T_s} & 0 & 0 & 0 \\ 0 & 0 & 0 & 1 & T_s & \Phi \\ 0 & 0 & 0 & 0 & 1 & \dfrac{(1 - e^{-\alpha T_s})}{\alpha} \\ 0 & 0 & 0 & 0 & 0 & e^{-\alpha T_s} \end{bmatrix} \tag{6}$$

where $\Phi = (e^{-\alpha T_s} + \alpha T_s - 1)/\alpha^2$, and α is a correlation parameter that models different classes of targets: a small α for targets with relatively slow maneuvers and a high α for targets with fast and evasive maneuvers. The details of the covariance matrix Q_k, the process noise η_k, and other characteristics of this model can be found in [27, 28].

In addition, this study assumes the UAVs are equipped with a GMTI sensor to localize the position of the target. Because the measurement of GMTI is composed of the range and azimuth of the target with respect to the radar location, the actual measurements are the relative range and azimuth with respect to the position of the airborne UAV. Note that in the present paper, the range rate measurement is not considered. The radar measurement $\mathbf{z}_k = (r_k, \phi_k)^T$ can be defined as the following nonlinear relation using the target position $(x_k^t, y_k^t)^T$ and the UAV position $(x_k, y_k)^T$ as:

$$\mathbf{z}_k = h(\mathbf{x}_k^t) + \boldsymbol{\nu}_k = \begin{pmatrix} \sqrt{(x_k^t - x_k)^2 + (y_k^t - y_k)^2} \\ \tan^{-1} \dfrac{y_k^t - y_k}{x_k^t - x_k} \end{pmatrix} + \boldsymbol{\nu}_k \tag{7}$$

where $\boldsymbol{\nu}_k$ is a measurement noise vector, and its noise covariance matrix is defined as:

$$V[\boldsymbol{\nu}_k] = R_k = \begin{bmatrix} \sigma_r^2 & 0 \\ 0 & \sigma_\phi^2 \end{bmatrix} \tag{8}$$

III. ROAD-CONSTRAINED TRACKING FILTER

To make use of road-map information for the estimation of a target traveling on a road, it is required to express the road map as a certain type of mathematical equation. This section first presents a road approximation algorithm using constant curvature segments and then applies it to one of the constrained estimations based on Kalman filtering along with decentralized sensor fusion using multiple UAVs.

A. Road Approximation Using Constant Curvature Segments

To generate the road using onboard sensor measurements or approximate the real road from a given road map, this study uses constant curvature segments. In this approach, assuming that some vertices on the road can be obtained, those vertices are connected by arc segments of constant curvature by introducing an intermediate point with C^1 contact (which represents that the first derivative is continuous), as shown in Fig. 1. The curved line (arc) between the two vertices represents the curved nature of the real road. The mathematical details of the construction of the curvature segments between vertices can be found in [29].

The entire road map can then be modelled by a set of road segments r_i, where $i \in \{1, \ldots, n_r\}$, and for each road segment, the center position of the curve and its curvature are given by the approximation algorithm. Fig. 2 illustrates the road approximation using the UAV sensor and constant curvature segments. As the UAV acquires some points on the road from the visual image sensor (marked as a cross

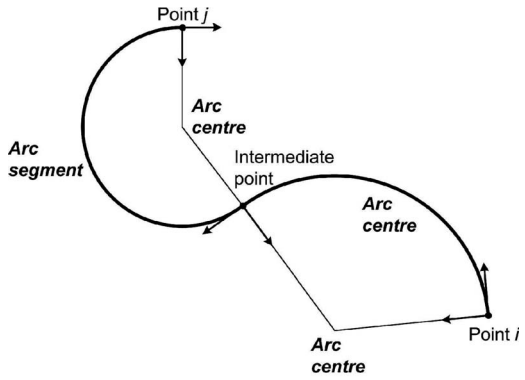

(a) Orientation 1

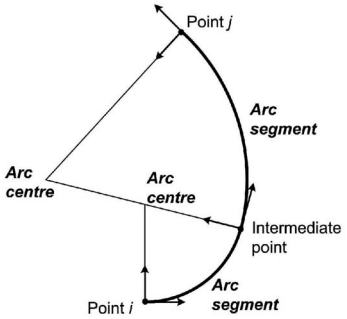

(b) Orientation 2

Fig. 1. Arc segments connecting two vertices with $\mathcal{C}^1$ contact at intermediate vertex. Two arc configurations are possible with same (orientation 2) or opposite (orientation 1) sign of curvature.

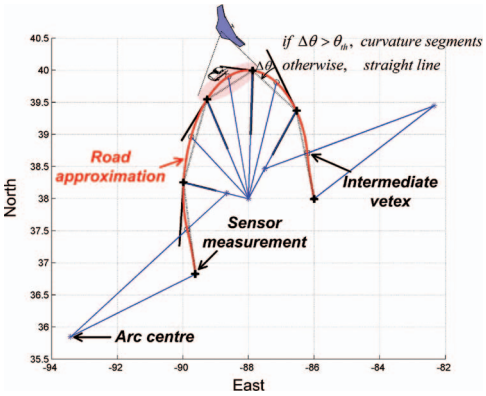

Fig. 2. Illustration of road approximation process using UAV visual sensor.

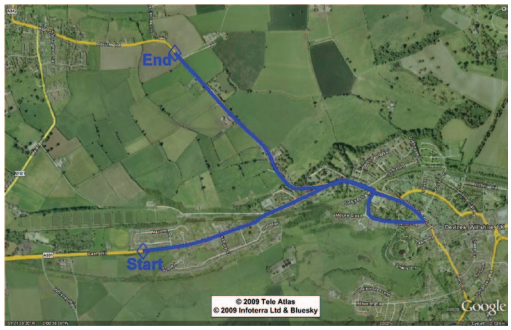

Fig. 3. Sample road network with GIS satellite data overlaid (Google Map).

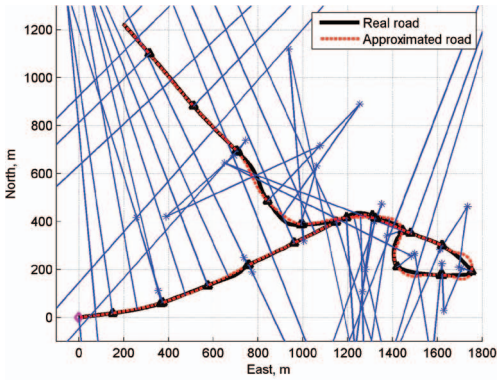

(a) Loosely represented roads

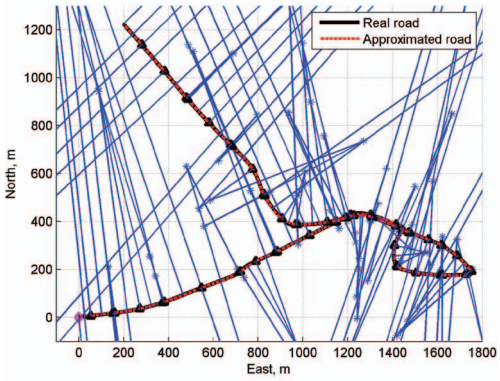

(b) Densely represented roads

Fig. 4. Road approximation using constant curvature segments.

in Fig. 2), the road is generated and extended successively. If a new point lies on or around the tangent line of a previous point, the road can be approximated as a straight line. Especially in the case that road information is not given in some area, the efficiency of this approach can be of interest, since only some of the points on the road and corresponding segment curvature by the algorithm are required to approximate roads quite close to real roads. This can be readily exploited for the precise estimation of the succeeding ground target on the road.

Fig. 3 shows a sample road network of Devizes, Wiltshire, United Kingdom, together with geographic information system (GIS) satellite data. Information for the road of interest, represented as the blue line, is assumed to be known in this study. Figs. 4–5 show the approximated road and curvature for each road segment using some of the known points on the road. Apparently, the more vertices that are used, the better is the fit to the road. However, since too many road segments might cause performance degradation in the constrained estimation, the appropriate number of vertices on the road needs to be determined to get a reasonable fit considering the road-network structure.

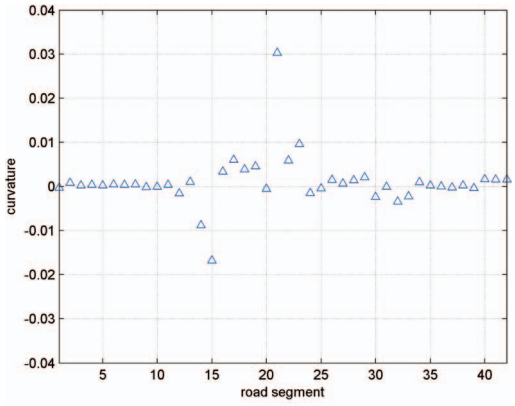

(a) Loosely represented roads

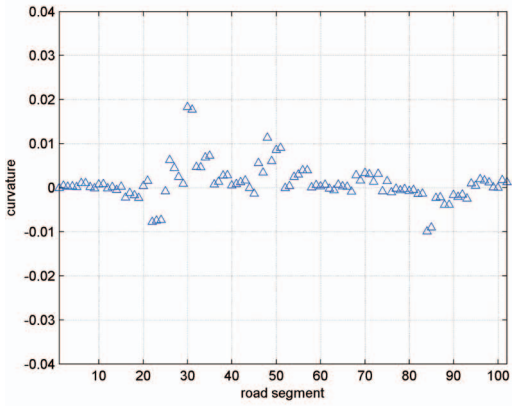

(b) Densely represented roads

Fig. 5. Curvature of each road segment.

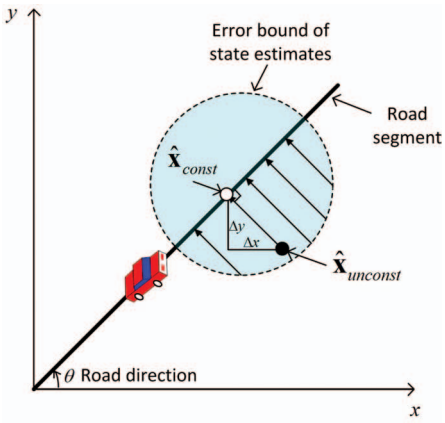

(a) Equality constraints

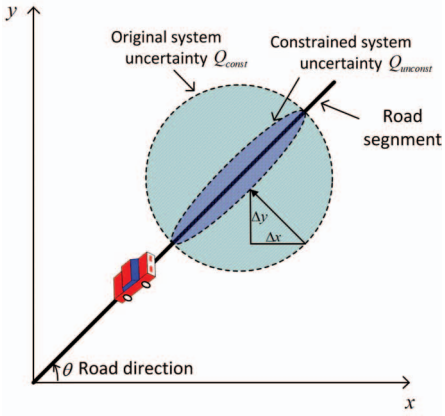

(b) Directional process noise

Fig. 6. Different ways to handle road constraints in constrained filtering framework.

B. Road-Constrained Estimation

Now, assuming that the ground vehicle moves along a given road map consisting of n_r road segments, the two-dimensional (2-D) position of the vehicle should lie on one of the segments. This can be expressed as the following constraint:

$$r_i(x_k^t, y_k^t) = 0 \tag{9}$$

where $r_i(\cdot)$ denotes the ith road segment, which can be modeled as a straight line, arc, or polynomials. For example, if the road is straight, the above road constraint can be expressed as:

$$r_i(x_k^t, y_k^t) = \tan\theta \cdot x_k^t - y_k^t = 0 \tag{10}$$

where θ is a given road direction. In this study, since the road is approximated using constant curvature segments, as explained earlier, the road constraint is obtained as:

$$r_i(x_k^t, y_k^t) = (x_k^t - x_{i,ct})^2 + (y_k^t - y_{i,ct})^2 - \left(\frac{1}{\kappa_i}\right)^2 = 0 \tag{11}$$

where $(x_{i,ct}, y_{i,ct})$ and κ_i are the center position and the curvature of the ith road segment, respectively.

Typically, there are two ways to deal with the road constraint in a constrained filtering framework. One is to use the road as equality constraints [12], and the other is to use the concept of a directional process noise [15], which represents uncertainty components along and orthogonal to the road, as illustrated in Fig. 6. In Fig. 6a, the error bound of a position estimate using conventional filtering with Gaussian noise is represented as a circle, and unconstrained estimate $\hat{\mathbf{x}}_{unconst}$ is projected onto the road, resulting in a better estimate $\hat{\mathbf{x}}_{const}$. In Fig. 6b, the process noise uncertainty Q_{const} is represented as an ellipsoid considering the higher motion uncertainty along the road and the smaller uncertainty orthogonal to the road, compared to Q_{unconst}, which is represented as a circle. This study uses a pseudomeasurement method, one of the constrained Kalman filtering algorithms, which treats the equality constraints as additional fictitious or pseudomeasurements [13]. Unlike other approaches, such as the maximum probability method and the projection method [11], this approach has the advantage of enabling consideration of the degree of constraint adherence, by monitoring the magnitude of the additional pseudomeasurement noise variance. The pseudomeasurement model using road constraints can be written as:

$$z_k^{r_i} = h_{r_i}(\mathbf{x}_k^t) + v_k^{r_i} \tag{12}$$

where $z_k^{r_i} = 0$, $h_{r_i}(\mathbf{x}_k^t) = r_i(\mathbf{x}_k^t)$, and $v_k^{r_i}$ is assumed to be a zero mean white Gaussian noise with covariance $R_k^{r_i} = (\sigma_r^{road})^2$, which accounts for the uncertainty of road constraints. Then, the previous real measurement model (7) is augmented by adding the pseudomeasurement to give:

$$\mathbf{z}_k^a = h_a(\mathbf{x}_k^t) + \boldsymbol{v}_k^a \tag{13}$$

where $\mathbf{z}_k^a = [\mathbf{z}_k \; z_k^{r_i}]^T$, $h_a(\mathbf{x}_k^t) = [h(\mathbf{x}_k^t) \; h_{r_i}(\mathbf{x}_k^t)]^T$, and $\boldsymbol{v}_k^a = [\boldsymbol{v}_k \; v_k^{r_i}]^T$. The measurement noise covariance is also augmented to be $R_k^a = \text{diag}(R_k, R_k^{r_i})$. Considering that $h_a(\mathbf{x}_k^t)$ is nonlinear, the localization of a target can be done by using the EKF with the augmented measurement equation, which will be called the measurement-augmented EKF (MAEKF), in the form:time update:

$$\mathbf{x}_{k|k-1}^t = F_k \mathbf{x}_{k-1|k-1}^t \tag{14}$$

$$P_{k|k-1}^t = F_k P_{k-1|k-1}^t F_k^T + Q_k \tag{15}$$

measurement update:

$$\upsilon_k = \mathbf{z}_k^a - h_a(\mathbf{x}_{k|k-1}^t) \tag{16}$$

$$S_k = H_k P_{k|k-1}^t H_k^T + R_k^a \tag{17}$$

$$\mathbf{x}_{k|k}^t = \mathbf{x}_{k|k-1}^t + P_{k|k-1}^t H_k^T S_k^{-1} \upsilon_k \tag{18}$$

$$P_{k|k}^t = (I - P_{k|k-1}^t H_k^T S_k^{-1} H_k) P_{k|k-1}^t \tag{19}$$

where the notation $k|k-1$ and $k|k$ represent a predicted state (and covariance) at time step k from the previous step $k-1$ and an updated state at time step k using the predicted state $k|k-1$, respectively. The output matrix H_k is a Jacobian of h_a with respect to the time-update state $\mathbf{x}_{k|k-1}^t$. As a target is moving from one road segment to another, an appropriate segment on which the target is traveling is selected, based on its estimated or a priori target position, its error covariance, and the road-network information as:

$$\begin{bmatrix} x_e^{r_i} - x_{k|k-1}^t \\ y_e^{r_i} - y_{k|k-1}^t \end{bmatrix}^T \left[P_{k|k-1}^{t,pos} \right]^{-1} \begin{bmatrix} x_e^{r_i} - x_{k|k-1}^t \\ y_e^{r_i} - y_{k|k-1}^t \end{bmatrix} < \varepsilon \tag{20}$$

where $(x_e^{r_i}, y_e^{r_i})$ is the end position of the ith road segment, ε is the gate threshold parameter, and $P_{k|k-1}^{t,pos}$ is the position submatrix of the prediction covariance $P_{k|k-1}^t$. Here, a current road segment is updated to the next segment once the above condition is satisfied.

In the case that nonlinearity of the road segment is severe, since the EKF based on linearization can result in poor performance, this study also designed the UKF, and we compared the results between those two filtering methods. Road constraints can be incorporated into the UKF by treating it as a pseudomeasurement in a similar way as in the EKF, but without linearization of constraints, which provides better accuracy. The UKF is a filter for nonlinear systems that uses sigma points approximating a given probability density function [30]. Among various UKF methods dealing with pseudomeasurements, an equality constrained UKF (ECUKF) is adopted in this study, considering its reasonable performance and computation time [31]. In the ECUKF, at each update step, the stated estimate of the unconstrained UKF is combined with the constraints, which are treated as pseudomeasurements, to obtain a constrained a posteriori UKF estimate. This constrained estimate is then used as the initial condition for the next time step.

C. Data Fusion for a Network of UAV Sensors

Since this study assumes that two UAVs carry out the cooperative standoff tracking of a ground moving target, each UAV's GMTI sensor can get its own measurement and execute the tracking filter algorithm separately. After each UAV receives the other's estimation via communication link, it can run a decentralized sensor fusion to enhance the tracking accuracy. This study simply adopts the following simple convex combination state-vector fusion [32], which is one of the simplest and easiest to implement state-vector fusion algorithms and assumes that the cross covariance between two track estimates can be ignored, and each individual track is independent [33, 34].

$$\hat{\mathbf{x}}_k^t = \mathbf{x}_{k|k}^t + P_{k|k}^t (P_{k|k}^t + P_{k|k}^p)^{-1} (\mathbf{x}_{k|k}^p - \mathbf{x}_{k|k}^t) \tag{21}$$

$$P_k^t = P_{k|k}^t - P_{k|k}^t (P_{k|k}^t + P_{k|k}^p)^{-1} P_{k|k}^{tT} \tag{22}$$

where $\mathbf{x}_{k|k}^p$ and $P_{k|k}^p$ represent the state and error covariance estimations of the pair of UAVs. It is assumed that the communication bandwidth is wide enough to transmit the state (6×1) and covariance matrices (6×6) in both directions between the pair of UAVs, and the clocks of the UAVs are synchronized for track-to-track fusion. Subsequently, $\hat{\mathbf{x}}_k^t$ in (21) will be used as the initial value of the state for the model prediction of a target for nonlinear model predictive control at each sampling point.

IV. MODEL PREDICTIVE COORDINATED STANDOFF TRACKING

The nonlinear model predictive coordinated standoff tracking (NMPCST) [25] decides a control input sequence for N sampling times:

$$U_k = \{\mathbf{u}_0, \mathbf{u}_1, \cdots, \mathbf{u}_{N-1}\} \tag{23}$$

that minimizes the following performance index for maintaining the distance between a UAV and a ground target as well as a relative phase angle between UAVs.

$$J = \phi(\tilde{r}_N, \tilde{d}_N) + \sum_{k=0}^{N-1} L(\tilde{r}_k, \tilde{d}_k, \mathbf{u_k}) \tag{24}$$

$$\phi(\tilde{r}_N, \tilde{d}_N) = \frac{1}{2}(p_r \tilde{r}_N^2 + p_d \tilde{d}_N^2) \tag{25}$$

$$L(\tilde{r}_k, \tilde{d}_k, \mathbf{u_k}) = \frac{1}{2}\left\{ q_r \tilde{r}_k + q_d \tilde{d}_k^2 + r_v \left(\frac{u_{vk} - v_0}{v_{max}} \right)^2 + r_\omega \left(\frac{u_{\omega k} - \frac{v_0}{r_d}}{\omega_{max}} \right)^2 \right\} \tag{26}$$

where

$$\tilde{r}_k = \frac{r_d^2 - |r_k|^2}{r_d^2} \tag{27}$$

$$\tilde{d}_k = \frac{r_k^T r_k^p + |r_k||r_k^p|}{r_d^2} \tag{28}$$

with $\boldsymbol{r}_k$ and $\boldsymbol{r}_k^p$ representing the relative vectors from the target position to the positions of the current UAV and its paired UAV, respectively, and where r_d is the desired standoff distance from the UAVs to the target position, v_0 is the nominal speed of the UAVs, and $\frac{v_0}{r_d}$ is the nominal angular velocity. Here, p_r, p_d, q_r, q_d, r_v, and r_ω are constant weighting scalars. The relative geometry between the UAV, the paired UAV, and the ground target is shown in Fig. 7.

In (28), $\tilde{d}_k$ is derived from the inner product of $\boldsymbol{r}_k$ and $\boldsymbol{r}_k^p$ as $\langle \boldsymbol{r}_k, \boldsymbol{r}_k^p \rangle = \boldsymbol{r}_k^T \boldsymbol{r}_k^p = |\boldsymbol{r}_k||\boldsymbol{r}_k^p| \cos \Delta\theta_k$, where $\Delta\theta_k = |\theta_k^p - \theta_k|$ with the phase angles of the UAV positions with respect to the current target location. If the phase difference $\Delta\theta_k$ is ideally maintained as π radian, the above equation is rearranged since $\cos\pi = -1$ as $\boldsymbol{r}_k^T \boldsymbol{r}_k^p + |\boldsymbol{r}_k||\boldsymbol{r}_k^p| = 0$. Therefore, if the left-hand side of the above equation is minimized, the maintenance of the phase angle can be achieved between a pair of UAVs [25]. To apply this technique to a different phase angle between UAVs other than 180 degrees, $\frac{1}{2} q_d \Delta\theta_k^2$ can be used instead of $\frac{1}{2} q_d \tilde{d}_k^2$. For example, to compensate for the measurement error in the azimuth of one UAV by the small range measurement error of the other UAV, a user can select 90 degrees as a target phase difference between the UAVs.

By incorporating the dynamics of the UAVs in (4) and admissible control input ranges described in (2)–(3) as equality and inequality constraints, an augmented performance index can be derived as:

$$\begin{aligned} J_a = \phi(\tilde{r}_N, \tilde{d}_N) + \sum_{k=0}^{N-1} \Big[& L(\tilde{r}_k, \tilde{d}_k, \mathbf{u}_k) \\ & + \lambda_{k+1}^T \{ f_d(\mathbf{x}_k, \mathbf{u}_k) - \mathbf{x}_{k+1} \} \\ & + \frac{1}{2}\mu_v l_{vk} S_v^2(\mathbf{u}_k) + \frac{1}{2}\mu_\omega l_{\omega k} S_\omega^2(\mathbf{u}_k) \Big] \end{aligned} \tag{29}$$

where $S_v(\mathbf{u}_k) = \frac{|u_{1k} - v_0| - v_{max}}{v_{max}} \leq 0$, $S_\omega(\mathbf{u}_k) = \frac{|u_{2k}| - \omega_{max}}{\omega_{max}} \leq 0$, λ_k is a Lagrange multiplier, and μ_v and μ_ω are penalty function parameters. Here, l_{vk}, and $l_{\omega k}$ are defined to avoid unnecessary computation for satisfying inequality constraints:

$$l_{*k} = \begin{cases} 0, & S_* \leq 0 \\ 1, & S_* > 0 \end{cases} \tag{30}$$

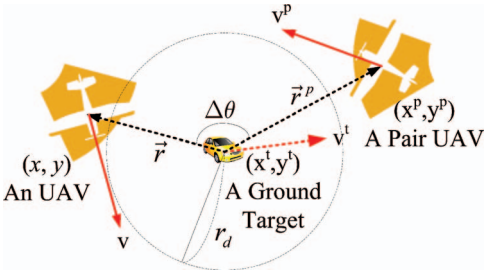

Fig. 7. Relative geometry between UAV, paired UAV, and ground target.

Let us define a Hamiltonian as:

$$\begin{aligned} M_k \triangleq & L(\tilde{r}_k, \tilde{d}_k, \mathbf{u}_k) + \lambda_{k+1}^T f_d(\mathbf{x}_k, \mathbf{u}_k) + \frac{1}{2}\mu_v l_{vk} S_v^2(\mathbf{u}_k) \\ & + \frac{1}{2}\mu_\omega l_{\omega k} S_\omega^2(\mathbf{u}_k) + \frac{1}{2}\mu_c l_{ck} S_c^2(\mathbf{x}_k) \end{aligned} \tag{31}$$

The variation of the augmented performance index is represented as:

$$\begin{aligned} dJ_a = & \left(\frac{\partial \phi(\tilde{r}_N, \tilde{d}_N)}{\partial \mathbf{x}_N} - \lambda_N^T \right) d\mathbf{x}_N + \sum_{k=1}^{N-1} \left[\left(\frac{\partial M_k}{\partial \mathbf{x}_k} - \lambda_k^T \right) d\mathbf{x}_k \right. \\ & \left. + \frac{\partial M_k}{\partial \mathbf{u}_k} d\mathbf{u}_k \right] + \frac{\partial M_0}{\partial \mathbf{x}_0} d\mathbf{x}_0 + \frac{\partial M_0}{\partial \mathbf{u}_0} d\mathbf{u}_0 \end{aligned} \tag{32}$$

By selecting the Lagrange multipliers as:

$$\lambda_N^T = \frac{\partial \phi(\tilde{r}_N, \tilde{d}_N)}{\partial \mathbf{x}_N} \tag{33}$$

$$\lambda_k^T = \frac{\partial M_k}{\partial \mathbf{x}_k} \quad \text{for } k = \mathrm{N} - 1, \ldots, 0 \tag{34}$$

the variation of J_a is changed to:

$$dJ_a = \sum_{k=0}^{N-1} \frac{\partial M_k}{\partial \mathbf{u}_k} d\mathbf{u}_k + \lambda_0^T d\mathbf{x}_0 \tag{35}$$

Substituting $d\mathbf{u}_k$ to minimize M_k into (35) as

$$d\mathbf{u}_k = -\Delta_k \frac{\partial M_k}{\partial \mathbf{u}_k}^T \tag{36}$$

gives the following decreasing variation of J_a.

$$dJ_a = -\sum_{k=0}^{N-1} \Delta_k \frac{\partial M_k}{\partial \mathbf{u}_k} \frac{\partial M_k}{\partial \mathbf{u}_k}^T + \lambda_0^T d\mathbf{x}_0 \tag{37}$$

Therefore, the control input can be updated using (36) as:

$$\mathbf{u}_k^{i+1} = \mathbf{u}_k^i - \Delta_k \frac{\partial M_k}{\partial \mathbf{u}_k}^T \text{ for } k = 0, \ldots, \mathrm{N} - 1 \tag{38}$$

where i is the index of iteration, and Δ_k is the step size. Derivation of the required Jacobians and definitions such as $\frac{\partial \phi(\tilde{r}_N, \tilde{d}_N)}{\partial \mathbf{x}_N}$ and $\frac{\partial M_k}{\partial \mathbf{u}_k}$ can be found in detail in [25].

Each UAV runs the above optimization routine in flight in a decentralized way at each sampling. When the measurement on the target comes in, each UAV performs the target localization and then shares the control/state of

TABLE I
Simulation Parameters

Parameter	Value	Unit
α	0.6	N/A
σ_a	0.66	m/s^2
θ_d	π	rad
v_0	40	m/s
r_d	500	m
r_c	30	m
v_{max}	10	m/s
ω_{max}	0.2	rad/s
τ_v, τ_ω	1/3	s
N	4 (equivalent to 2 s)	N/A
$(p_r, p_d, q_r, q_d, r_v, r_\omega)$	$(2e5, 1e6, p_r/N, p_d/N, 1e2, 5e1)$	N/A
μ_v, μ_ω	$1e3$	N/A
ε	0.8	N/A

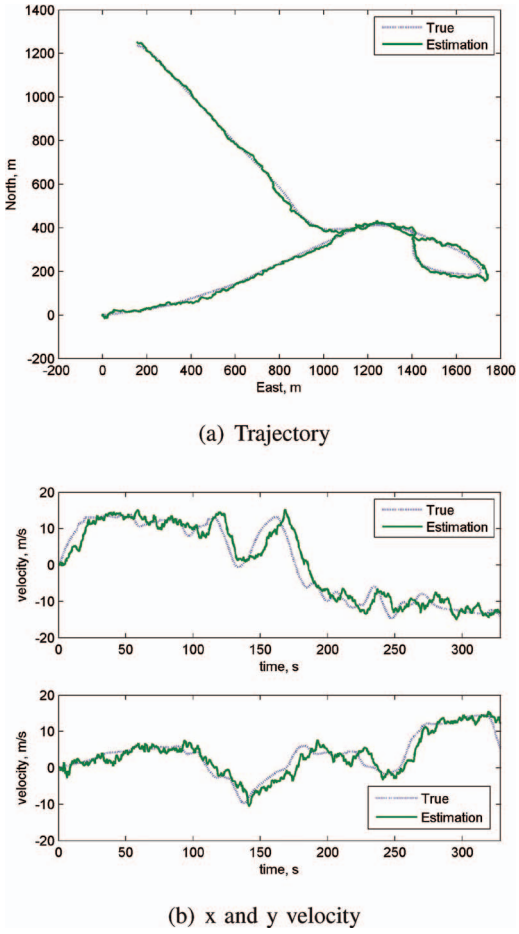

(a) Trajectory

(b) x and y velocity

Fig. 8. State-vector fusion results based on EKF.

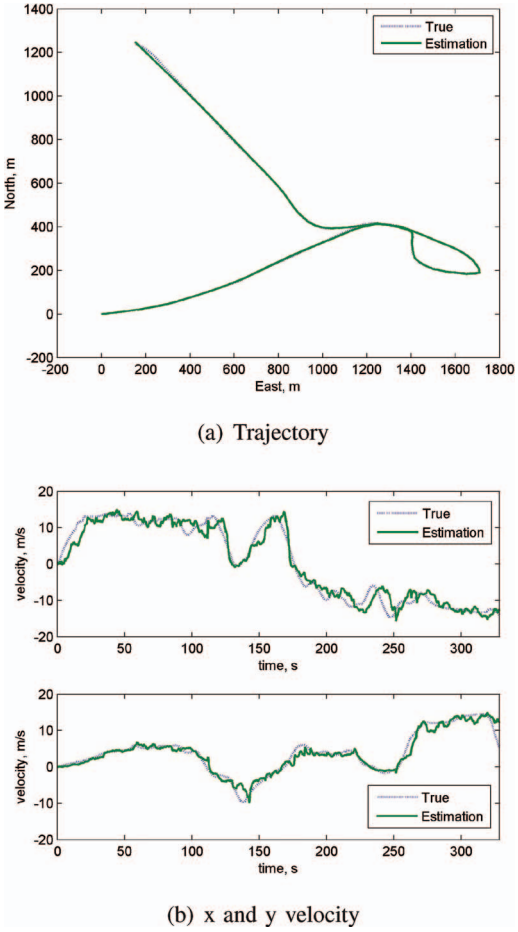

(a) Trajectory

(b) x and y velocity

Fig. 9. State-vector fusion results based on road-constrained ECUKF.

the UAVs and their state/covariance estimation information of the target via communications.

V. NUMERICAL SIMULATIONS

This section carries out numerical simulations using the proposed road-map–assisted NMPCST for a moving ground vehicle. The vehicle trajectory data, acquired at 2 Hz from an S-Paramics [35] traffic model using the Devizes map as previously shown in Fig. 3, are used to generate the GMTI measurements, composed of relative range and azimuth angle with respect to the position of the UAV. Generated GMTI measurements of a pair of UAVs were mixed with the white noise having the following standard deviations: UAV1 $(\sigma_r, \sigma_\phi) = (20$ m, 7 degrees) and UAV2 $(\sigma_r, \sigma_\phi) = (30$ m, 5 degrees). Note that false alarms and missed detection in low Doppler or cluttered areas for the GMTI sensor are considered in this study. For performance analysis, we used Monte Carlo simulations with a hundred independent runs and then averaged the results, unless otherwise stated. The other parameters needed for NMPCST can be found in Table I.

First, Figs. 8–9 display the estimated position and velocity of a ground target using the state-vector fusion based on the EKF and the road-constrained ECUKF, respectively, from single run results. Table II shows the mean tracking errors in position and velocity among different filtering methods. Apparently, the EKF and the UKF using the decentralized sensor fusion based on the state-vector fusion of two UAVs shows better performance than that using only a single UAV, and the road-constrained ECUKF with data fusion provides the best estimation accuracy. In addition, Figs. 10–12 display NMPCST simulation results, including the relative

TABLE II
Performance Comparison with Different Estimation Methods Averaged Over a Hundred Monte Carlo Simulations

	Single UAV		Multiple UAVs (State-Vector Fusion)			
	Unconstrained		Unconstrained		Road-Constrained	
Mean error	$EKF_{UAV,1}$	$EKF_{UAV,2}$	EKF_{multi}	UKF_{multi}	$MAEKF_{multi,c}$	$ECUKF_{multi,c}$
Position (m)	20.7141	17.5897	14.4868	14.2238	7.7811	7.3599
Velocity (m/s)	3.7757	3.4465	3.2418	3.3099	2.1498	2.0651

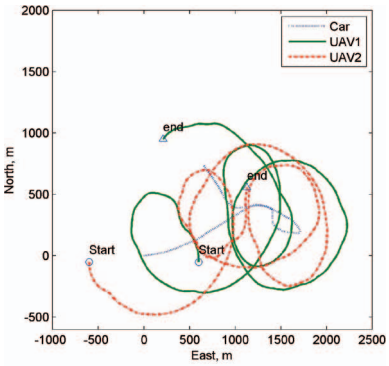

(a) Absolute trajectories

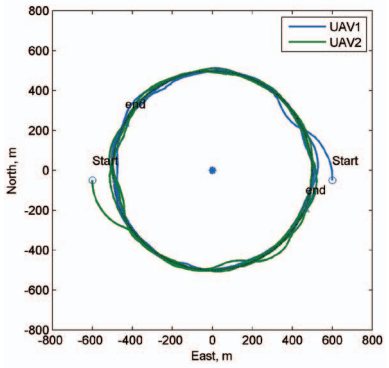

(b) Relative trajectories of UAVs

Fig. 10. Nonlinear model predictive standoff tracking simulations results.

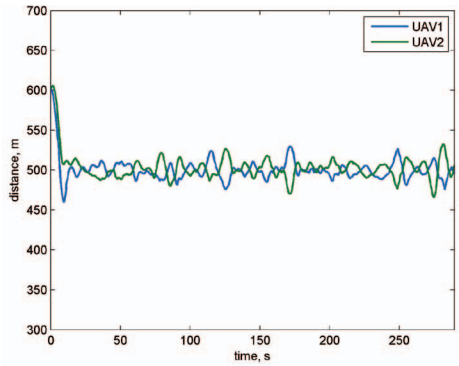

(a) Standoff distance evolution

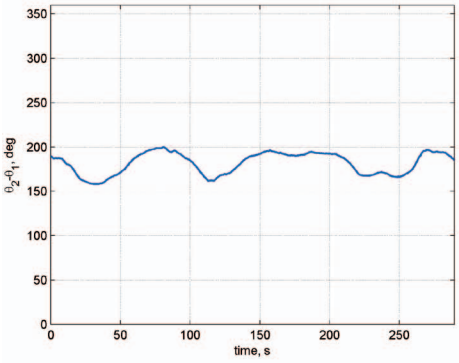

(b) Phase angle difference of UAVs

Fig. 11. Nonlinear model predictive standoff tracking simulations results.

trajectories of the UAVs with respect to the ground vehicle, standoff tracking error, phase angle difference between UAVs, and control input histories. Note that high-frequency control inputs are required to be followed by the UAVs for both velocity and turning rate, which are hard to achieve in practice. Even though actuator time delay (τ_v, τ_ω) in a UAV kinematic model is used in order to simulate this effect, more detailed control requirements will be investigated in future work.

To verify the feasibility and benefits of the proposed approach, the same scenarios explained above were tested for broadly used LVFG [19] as well as NMPCST. Here, the LVFG uses a decoupled one-step feedback control structure [19]: the heading control for maintenance of standoff distance, which guides the UAV onto the generated stable orbit around a target, and the speed control for phase angle maintenance on the same orbit. Meanwhile, the NMPC guidance utilizes the coupled optimal control commands computed over the receding horizon time steps, thus relying more on the target estimation accuracy. Table III compares tracking guidance performance for standoff distance and phase keeping between LVFG and NMPCST using either the EKF or the road-constrained ECUKF. It is worthwhile to note that the performance improvement of NMPCST with changing estimation method from the EKF to the ECUKF is more remarkable than that of LVFG, since NMPCST uses predicted target information to a certain future time explicitly.

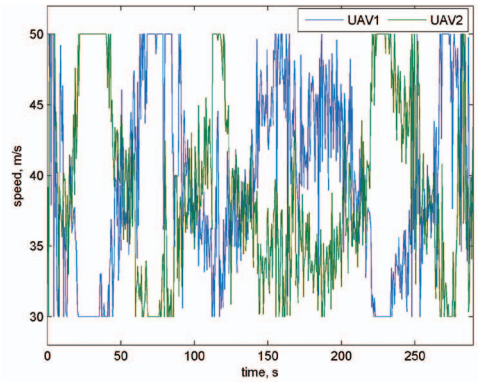

(a) Control input of UAVs: u_v

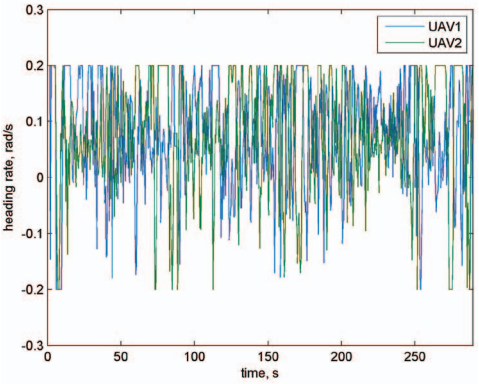

(b) Control input of UAVs: u_ω

Fig. 12. Nonlinear model predictive standoff tracking simulations results.

TABLE III
Tracking Performance with Different Estimation Methods Averaged Over a Hundred Monte Carlo Simulations

	LVFG		NMPCST	
Mean error	EKF_{multi}	$ECUKF_{multi,c}$	EKF_{multi}	$ECUKF_{multi,c}$
Standoff distance (m)	16.0767	12.9999	13.4243	9.5025
Phase keeping (deg)	13.0413	12.8627	12.5695	11.1718

VI. CONCLUSIONS AND FUTURE WORK

This paper has presented the road-map–assisted standoff tracking of a moving ground vehicle using nonlinear model predictive control, and particularly focused on using road-map information to enhance target estimation accuracy. First, a practical road approximation algorithm was proposed using constant curvature segments, and to exploit road information for precise tracking of a target, nonlinear road-constrained Kalman filtering using a pseudomeasurement approach was applied. To address nonlinearity of road constraints and provide good estimation performance, both the EKF and the UKF were implemented along with the state-vector fusion technique. In the numerical simulation results as to standoff target tracking, the effect of improved estimation accuracy on the tracking guidance performance was analyzed for both LVFG and the proposed NMPC guidance. In brief, this study verified the impact of the proposed approach on the standoff tracking guidance performance, and this can be a foundation technique for intelligence, surveillance, target acquisition, and reconnaissance (ISTAR) applications in military and police enforcement domains.

Extension of the proposed road-constrained filtering to the variable structure IMM filter concept [14, 15] will be followed as future work, which can consider multiple roads at junctions and different vehicle models to assign the target to the corresponding road segment correctly when there are ambiguities or unreliable sensor measurements. Additionally, more options for the phase angle difference between UAVs, including 90 degrees, will be tested for obtaining better coordinated estimation performance.

ACKNOWLEDGMENTS

This study was supported by 1) the UK Engineering and Physical Science Research Council (EPSRC) under the Grant EP/J011525/1 and 2) “Guidance/Control Study for Take-off and Landing on a Ship” program through the Agency for Defense Development (ADD) of KOREA (UD1130053JD).

REFERENCES

[1] Kim, M., and Kim, Y.
Multiple UAVs nonlinear guidance laws for stationary target observation with waypoint incidence angle constraint.
International Journal of Aeronautical and Space Sciences, **14**, 1 (2013), 67–74.

[2] Oh, H., Kim, S., Shin, H., Tsourdos, A., and White, B. A.
Behaviour recognition of ground vehicle using airborne monitoring of unmanned aerial vehicles.
International Journal of Systems Science, **45**, 12 (2013), 2499–2514. DOI:10.1080/00207721.2013.772677.

[3] Yoon, S., Park, S., and Kim, Y.
Circular motion guidance law for coordinated standoff tracking of a moving target.
IEEE Transactions on Aerospace and Electronic Systems, **49**, 4 (2013), 2440–2462.

[4] Koch, W., Koller, J., and Ulmke, M.
Ground target tracking and road map extraction.
ISPRS Journal of Photogrammetry and Remote Sensing, **61**, 3–4 (2006), 197–208.

[5] Tang, Z., and Ozguner, U.
Sensor fusion for target tracking maintenance with multiple UAVs based on Bayesian filtering method and hospitability map.
In *Proceedings of the 42nd IEEE Conference on Decision and Control*, Maui, Hawaii, USA, Dec. 2003.

[6] Kanchanavally, S., Ordonez, R., and Layne, J.
Mobile target tracking by networked uninhabited autonomous vehicles via hospitability maps.
In *Proceedings of the 2004 American Control Conference*, Boston, MA, Jun.–Jul. 2004.

[7] Kassas, Z. M., and Ozguner, U.
A nonlinear filter coupled with hospitability and synthetic inclination maps for in-surveillance and out-of-surveillance tracking.
IEEE Transactions on Systems, Man, and Cybernetics–Part C: Application and Reviews, **40**, 1 (2010), 87–97.

[8] Ulmke, M., and Koch, W.
Road-map assisted ground moving target tracking.
IEEE Transactions on Aerospace and Electronic Systems, **42**, 4 (2006), 1264–1274.

[9] Streller, D.
Road map assisted ground target tracking.
In *Proceedings of the 11th International Conference on Information Fusion*, Cologne, Germany, Jun.–Jul. 2008.

[10] Herrero, J. G., Portas, J. A. B., and Corredera, J. R. C.
Use of map information for tracking targets on airport surface.
IEEE Transactions on Aerospace and Electronic Systems, **39**, 2 (2003), 675–693.

[11] Simon, D., and Chia, T. L.
Kalman filtering with state equality constraints.
IEEE Transactions on Aerospace and Electronic Systems, **38**, 1 (2002), 128–136.

[12] Zhang, M., Knedik, S., and Loffeld, O.
An adaptive road-constrained IMM estimator for ground target tracking in GSM networks.
In *Proceedings of the 10th International Conference on Information Fusion*, Quebec, Canada, Jul. 2007.

[13] Tahk, M., and Speyer, J. L.
Target tracking problems subject to kinematic constraints.
IEEE Transactions on Automatic Control, **35**, 3 (1990), 324–326.

[14] Kirubarajan, T., Bar-Shalom, Y., Pattipati, K. R., and Kadar, I.
Ground target tracking with variable structure IMM estimator.
IEEE Transactions on Aerospace and Electronic Systems, **36**, 1 (2000), 26–46.

[15] Arulampalam, M. S., Gordon, N., Orton, M., and Ristic, B.
A variable structure multiple model particle filter for GMTI tracking.
In *Proceedings of the 5th International Conference on Information Fusion*, Annapolis, MD, Jul. 2002.

[16] Arulampalam, M. S., Maskell, S., Gordon, N., and Clapp, T.
A tutorial on particle filters for online nonlinear/non-Gaussian Bayesian tracking.
IEEE Transactions on Signal Processing, **50**, 2 (2002), 174–188.

[17] Ristic, B., Arulampalam, S., and Gordon, N.
Beyond the Kalman Filter: Particle Filters for Tracking Applications. London: Artech House Publishers, 2004.

[18] Lawrence, D. A.
Lyapunov vector fields for UAV flock coordination.
In *2nd AIAA Unmanned Unlimited Conference, Workshop, and Exhibit*, Reston, VA, Sep. 2003.

[19] Frew, E. W., Lawrence, D. A., and Morris, S.
Coordinated standoff tracking of moving targets using Lyapunov guidance vector fields.
Journal of Guidance, Control, and Dynamics, **31**, 2 (2008), 290–306.

[20] Morris, S., and Frew, E. W.
Cooperative tracking of moving targets by teams of autonomous unmanned air vehicles.
Arlington, VA: MLB Company, Technical Report FA9550-04-C-0107, 2005.

[21] Summers, T. H., Akella, M. R., and Mears, M. J.
Coordinated standoff tracking of moving targets: Control laws and information architectures.
Journal of Guidance, Control, and Dynamics, **32**, 1 (2009), 56–69.

[22] Kingston, D., and Beard, R.
UAV splay state configuration for moving targets in wind.
Lecture Notes in Control and Information, **369** (2007), 109–128.

[23] Oh, H., Kim, S., Shin, H. S., White, B. A., Tsourdos, A., and Rabbath, C. A.
Rendezvous and standoff target tracking guidance using differential geometry.
Journal of Intelligent and Robotic Systems, **69**, 1–4 (2013), 389–405.

[24] Oh, H., Kim, S., Shin, H.-S., Tsourdos, A., and White, B.
Coordinated standoff tracking of groups of moving targets using multiple UAVs.
In *21st Mediterranean Conference on Control and Automation*, Crete, Greece, June 2013.

[25] Kim, S., Oh, H., and Tsourdos, A.
Nonlinear model predictive coordinated standoff tracking of a moving ground vehicle.
Journal of Guidance, Control, and Dynamics, **36**, 2 (2013), 557–566.

[26] Wise, R. A., and Rysdyk, R. T.
UAV coordination for autonomous target tracking.
In *AIAA Guidance, Navigation and Control Conference*, Keystone, CO, Aug. 2006.

[27] Mehrotra, K., and Mahapatra, P. R.
A jerk model for tracking highly maneuvering targets.
IEEE Transactions on Aerospace and Electronic Systems, **33**, 4 (1997), 1094–1105.

[28] Bar-Shalom, Y., Li, X. R., and Kirubarajan, T.
Estimation with Applications to Tracking and Navigation: Theory, Algorithms, and Software. New York: John Wiley & Sons, 2001.

[29] White, B. A., Tsourdos, A., Ashokaraj, I., Subchan, S., and Zbkowski, R.
Contaminant cloud boundary monitoring using network of UAV sensors.
IEEE Sensors Journal, **8**, 10 (2008), 1681–1692.

[30] Julier, S. J., and Uhlmann, J. K.
A new extension of the Kalman filter to nonlinear systems.
In *Proceedings of AeroSense: 11th International Symposium on Aerospace/Defense Sensing, Simulation and Controls*, Orlando, FL, Apr. 1997, 182–193.

[31] Simon, D.
Kalman filtering with state constraints: A survey of linear and nonlinear algorithms.
IET Control Theory and Applications, **4**, 8 (2010), 1303–1318.

[32] Brooks, R. R., and Iyengar, S. S.
Multi-sensor Fusion: Fundamentals and Applications with Software. Upper Saddle River, NJ: Prentice Hall, 1997.

[33] Ng, G. W., Tan, C. H., and Ng, T. P.
Tracking ground targets using state vector fusion.
In *Proceedings of the 8th International Conference on Information Fusion*, Philadelphia, PA, Jul. 2005.

[34] Roecker, J. A., and McGillem, C. D.
Comparison of two-sensor tracking methods based on state vector fusion and measurement fusion.
IEEE Transactions on Aerospace and Electronic Systems, **24**, 4 (1988), 447–449.

[35] *S-Paramics Software*. SIAS Limited, http://www.sias.com, Jan 2011.

Hyondong Oh received B.Sc. and M.Sc. degrees in aerospace engineering from Korea Advanced Institute of Science and Technology (KAIST), South Korea, in 2004 and 2010, respectively, and then he acquired a Ph.D. degree in autonomous surveillance and target tracking guidance using multiple UAVs from Cranfield University, United Kingdom, in 2013. He worked as a postdoctoral research associate on EC FP7 project "SWARM-ORGAN" at Nature Inspired Computing and Engineering (NICE) Group, University of Surrey, United Kingdom. He is currently a lecturer in autonomous unmanned vehicles at Loughborough University, United Kingdom.

Seungkeun Kim received a B.Sc. degree in mechanical and aerospace engineering from Seoul National University (SNU), Seoul, Korea, in 2002, and then acquired a Ph.D. degree from SNU in 2008. He is currently an assistant professor at the Department of Aerospace Engineering, Chungnam National University, Korea. Previously he was a research fellow and a lecturer at Cranfield University, United Kingdom, in 2008–2012. He has published book chapters, journal articles, and conference papers related to unmanned systems. His research interests cover nonlinear guidance and control, estimation, sensor and information fusion, fault diagnosis, fault tolerant control, and decision making for unmanned systems.

Antonios Tsourdos obtained an M.Eng. in electronic, control, and systems engineering from the University of Sheffield (1995), an M.Sc. degree in systems engineering from Cardiff University (1996), and a Ph.D. degree in nonlinear robust missile autopilot design and analysis from Cranfield University (1999). He is a professor of control engineering at Cranfield University, appointed as the head of the Centre for Cyber-Physical Systems in 2013. Professor Tsourdos was a member of Team Stellar, the winning team for the United Kingdom Ministry of Defence (MoD) Grand Challenge (2008) and the Institution of Engineering and Technology (IET) Innovation Award (Category Team, 2009).

2015-04-30

Road-map-assisted standoff tracking of moving ground vehicle using nonlinear model predictive control

Oh, Hyondong

IEEE

Hyondong Oh, Seungkeun Kim and Antonios Tsourdos, Road-map-assisted standoff tracking of moving ground vehicle using nonlinear model predictive control. IEEE Transactions on Aerospace and Electronic Systems, 2015, Vol. 51, Iss. 2, pp975-986

http://dx.doi.org/10.1109/TAES.2014.130688